Projected Future Changes in the Equatorial Wave Spectrum in CMIP6

Hagar Bartana (haggarb@gmail.com)
Hebrew University of Jerusalem Fredy and Nadine Herrmann Institute of Earth Sciences
https://orcid.org/0000-0002-4278-4590
Chaim I. Garfinkel
Hebrew University of Jerusalem Fredy and Nadine Herrmann Institute of Earth Sciences
Ofer Shamir
New York University Courant Institute of Mathematical Sciences
Jian Rao
Nanjing University of Information Science and Technology

Research Article

Keywords: Convectively coupled equatorial waves, CMIP, Kelvin waves, Madden Julian Oscillation, Tropical spectrum

Posted Date: June 3rd, 2022

DOI: https://doi.org/10.21203/rs.3.rs-1064219/v2

Climate Dynamics manuscript No.
(will be inserted by the editor)

Projected Future Changes in Equatorial Wave Spectrum in CMIP6

Hagar Bartana · Chaim I. Garfinkel · Ofer Shamir · Jian Rao

Received: date / Accepted: date

Abstract The simulation of the Madden-Julian Oscillation (MJO) and convectively coupled equatorial waves (CCEWs) is considered in 13 state-of-the-art models from phase 6 of the Coupled Model Intercomparison Project (CMIP6). We use frequency-wavenumber power spectra of the models and observations for Outgoing Longwave Radiation (OLR) and zonal winds at 250 hPa (U250), and consider the historical simulations and end of 21st century projections for the SSP245 and SSP585 scenarios.

The models simulate a spectrum quantitatively resembling that observed, though systematic biases exist. MJO and Kelvin waves (KW) are mostly underestimated, while equatorial Rossby waves (ER) are overestimated. Most models project a future increase in power spectra for the MJO, while nearly all project a robust increase for KW and weaker power values for most other wavenumber-frequency combinations, including higher wavenumber ER. In addition to strengthening, KW also shift toward higher phase speeds (or equivalent depths). Models with a more realistic MJO in their control climate tend to simulate a stronger future intensification.

Chaim I. Garfinkel
The Fredy and Nadine Herrmann Institute of Earth Sciences, Hebrew University of Jerusalem, Jerusalem, Israel
E-mail: chaim.garfinkel@mail.huji.ac.il

Ofer Shamir
Center for Atmosphere-Ocean Science, Courant Institute of Mathematical Sciences, New York, New York

Jian Rao
Key Laboratory of Meteorological Disaster, Ministry of Education (KLME)/Joint International Research Laboratory of Climate and Environment Change (ILCEC)/Collaborative Innovation Center on Forecast and Evaluation of Meteorological Disasters (CIC-FEMD), Nanjing University of Information Science and Technology, Nanjing, China

Hagar Bartana
The Fredy and Nadine Herrmann Institute of Earth Sciences, Hebrew University of Jerusalem, Jerusalem, Israel

Keywords Convectively coupled equatorial waves · CMIP · Kelvin waves · Madden Julian Oscillation · Tropical spectrum

1 Introduction

The Madden-Julian Oscillation (MJO) is the dominant mode of intraseasonal (1-3 months) variability in the tropical atmosphere (Le et al, 2021; Jiang et al, 2020; Ahn et al, 2017; Hung et al, 2013; Zhang, 2005; Madden and Julian, 1972). It is characterized by eastward-propagating, planetary-scale envelopes of convective cloud clusters that are tightly coupled with the large-scale wind field. Its large spatial extent and low frequency (zonal wavenumbers 1-3 and 30-90 days period) distinguishes it from convectively coupled equatorial waves (CCEWs) and other disturbances (Le et al, 2021; Ahn et al, 2020; Jiang et al, 2020; Ahn et al, 2017; Hung et al, 2013).

CCEWs are manifested as equatorially trapped, zonally propagating tropical circulations, and comprise a non-negligible fraction of sub-monthly tropical dynamical and convective variability. The CCEWs include Kelvin waves (KW), equatorial Rossby (ER), mixed Rossby-gravity (MRG), eastward inertio-gravity (EIG), and westward inertio-gravity (WIG) waves (Huang et al, 2013; Hung et al, 2013; Seo et al, 2012; Kiladis et al, 2009; Wheeler and Kiladis, 1999).

The MJO and CCEWs interact with a wide range of tropical weather and climate phenomena, including monsoonal systems, tropical cyclone activity, and the El Niño-Southern Oscillation (Le et al, 2021; Ahn et al, 2017; Hung et al, 2013). Furthermore, they also exhibit teleconnections to the extratropics, affecting regional hydroclimate, and influencing weather and climate phenomena in the mid-latitude and high-latitude regions (Le et al, 2021; Ahn et al, 2020; Schwartz and Garfinkel, 2020; Raghavendra et al, 2019; Ahn et al, 2017; Hung et al, 2013; Yoo et al, 2012). Therefore, they play an important role in the global climate system, and are a key source of predictability for extended-range forecasts in both the tropics and extratropics (Rao et al, 2021, 2020, 2019; Jiang et al, 2020; Raghavendra et al, 2019; Hung et al, 2013; Kiladis et al, 2009; Zhang, 2005).

The ability of state-of-the-art coupled general circulation models to accurately capture the MJO's magnitude, location, and dynamics is of vital importance for subseasonal-to-seasonal prediction (Le et al, 2021; Raghavendra et al, 2019; Jiang et al, 2020; Vitart, 2017; Stan et al, 2022). A wide range of factors, for example - air-sea coupling, vertical heating profile and cloud parameterization - have been shown to influence the strength of the MJO and CCEWs in models (Le et al, 2021; Ahn et al, 2020, 2017; Hung et al, 2013; Wang and Li, 2017; Raghavendra et al, 2019; Seo et al, 2012; Jiang et al, 2015; Huang et al, 2013; Jiang et al, 2020; Lin et al, 2006).

Despite the importance of the MJO, very few models from earlier phases, including phase 5 of the Coupled Model Intercomparison Project (CMIP), were able to simulate a realistic MJO (Raghavendra et al, 2019; Lin et al, 2006). Although only a few studies have investigated the performance of CMIP6 models in capturing CCEWs and the MJO so far, there seems to be a robust improvement in the representation of MJO in the CMIP6 models. Specifically, CMIP6 models with an improved representation of convection show significantly better results (Ahn et al, 2020). Nevertheless, they still tend to underestimate the variability contributed by the MJO (Le et al, 2021; Ahn et al, 2020), even as they exhibit reasonable spectral power or total variance within the intraseasonal timescales as compared to observations.

While acknowledging the limitations of the models, they allow us a glimpse of future change possibilities. Previous work predicts an intensification of the MJO and KW, more tropical precipitation, and more intense convection, in response to increased greenhouse gas concentrations (Bui and Maloney, 2019; Maloney et al, 2019; Raghavendra et al, 2019; Chang et al, 2015). However, the intensification of MJO related zonal wind anomalies in the upper troposphere is unclear (Maloney et al, 2019), perhaps because the overall convective mass flux is expected to weaken, even as precipitation strengthens (Allan et al, 2020; Held and Soden, 2006). These upper tropospheric wind anomalies are of crucial importance for the upper level divergence anomalies that force teleconnections (Seo and Lee, 2017). By the end of the century the MJO might have less influence on extratropical phenomena in some regions (Bui and Maloney, 2019; Chang et al, 2015), while the influence in others such as the North Atlantic might be stronger (Samarasinghe et al, 2021).

In this study, we analyze the ability of 13 CMIP6 models to represent the MJO and CCEWs in the current climate, and then analyze their future projections. We specifically focus on the KW and ER, as they are strongly associated with the MJO and have strong mutual influence.

Section 2 will describe the data and methods. The results (section 3) are divided into two subsections: analysis of historical biases, and an analysis of future assessments. Discussion and conclusions are presented in section 4.

2 Data and Methods

2.1 Data

Thirteen CMIP6 models are analyzed in this study, chosen based on the availability of daily data for outgoing long wave radiation (OLR) and zonal winds at 250 hPa (U250) for both the historical scenario and the two future scenarios: SSP245 and SSP585. The SSP585 scenario includes an additional radiative forcing of 8.5 W/m^2 by the year 2099 while the SSP245 scenario includes an additional radiative forcing of 4.5 W/m^2 by the year 2099 (Meinshausen et al, 2020). Historical simulations are compared to observational data according to the relevant parameter: OLR updated from NOAA (Liebmann and Smith, 1996) and U250 from ERA5 (Hersbach et al, 2020). The years used for the historical data are 1979-2009, and years used for future assessments are 2069-2099. The OLR observational data has enhanced power around $(k, \omega) = (14, 0.1)$ that is likely an artifact of the sampling of the polar-orbiting

Table 1: Data products used

	data source	reference
obs.	NOAA OLR	Liebmann and Smith (1996)
	ERA-5	Hersbach et al (2020)
CMIP6	BCC-CSM2-MR	Wu et al (2019)
	CESM2	Danabasoglu et al (2020)
	CNRM-CM6-1	Voldoire et al (2019)
	CNRM-ESM2-1	Séférian et al (2019)
	EC-Earth3	Döscher et al (2021)
	FGOALS-g3	Li et al (2020)
	GFDL-CM4	Dunne et al (2020)
	INM-CM4-8	Volodin et al (2017)
	INM-CM5-0	Volodin et al (2017)
	MIROC6	Tatebe et al (2019)
	MPI-ESM1-2-HR	Müller et al (2018)
	MPI-ESM1-2-LR	Mauritsen et al (2019)
	UKESM1-0-LL	Sellar et al (2019)

Table 1 The data sources used in this study.

satellites (Wheeler and Kiladis, 1999). This area is not associated with either the MJO or any of the CCEWs so we ignore it. Table 1 summarizes the data products used. Further information about the models can be found in Online Resource 1.

We focus on OLR and U250 for two reasons. OLR allows us to compare to previous work using earlier CMIP generations and also to observations (Le et al, 2021; Raghavendra et al, 2019). We focus also on U250 because of its relationship with upper level divergence. Upper level divergence and divergent outflow lead to teleconnections in mid-latitudes (Sardeshmukh and Hoskins, 1988; Hoskins and Karoly, 1981), and hence an increase, say, in MJO activity of U250 may be expected to lead to stronger or more frequent teleconnections. Exploring this possibility is left for future work, and in particular we note the recent study of Jenney et al (2021) who find that changes in the subtropical mean state may be more important than changes in the MJO itself for future changes in MJO teleconnections.

2.2 Methods

We use the open-source wkSpaceTime routine of the NCAR Command Language, which implements the analysis described in Wheeler and Kiladis (1999) without the tropical depression filter used in Kiladis et al (2009). The results of the following sections were obtained using a temporal window of 96 days with an overlap of 10 days between consecutive windows, and a meridional window of $15°S - 15°N$. We overlay on the spectra the theoretical dispersion relations obtained by Matsuno (1966) for equivalent depths of 10m, 30m and 90m, as differences between the β plane solutions of Matsuno and the exact spherical solutions are small for the parameter regime of Earth's tropics (Garfinkel et al, 2017; Paldor, 2015; Paldor et al, 2013).

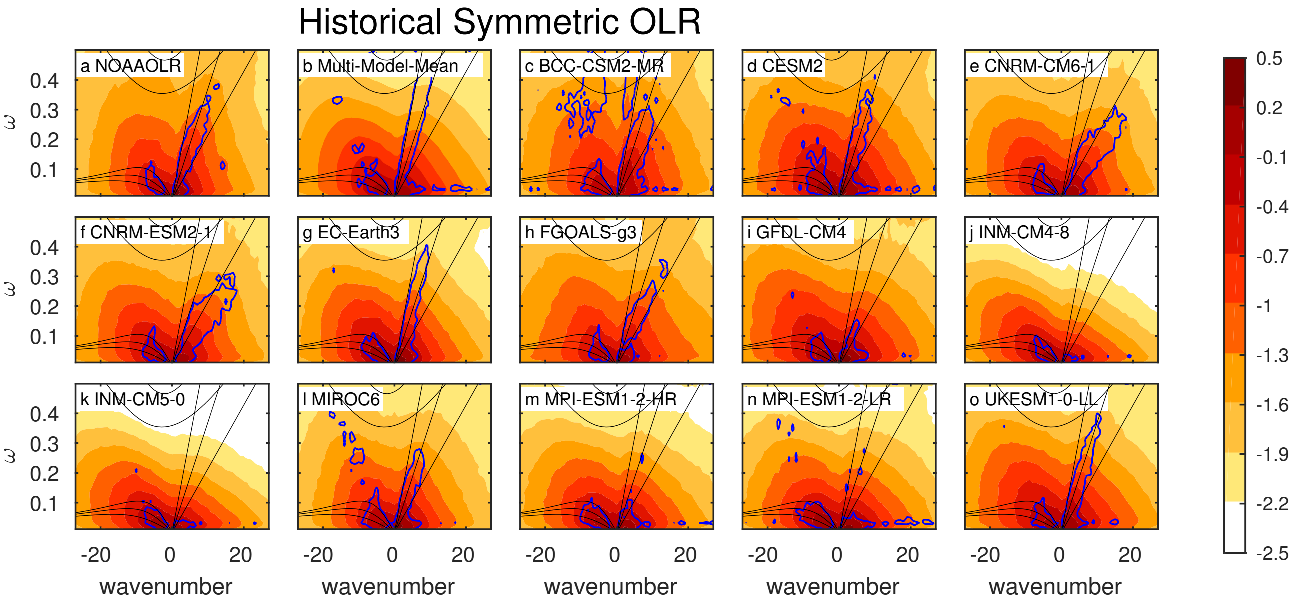

Fig. 1 $\log_{10}$ of the ω-k power spectra of the symmetric component of raw OLR $(W/m^2)^2 \cdot s$ data for all models and observations: (a) OLR observations, (b) MMM, and (c-o) individual models. Contour interval is 0.3. Black lines are the dispersion curves of equatorial waves for equivalent depths of 10m, 30m and 90m. A blue contour indicates where the power exceeds the background by 20%.

All data are processed and presented using a wavenumber-frequency (ω-k) power spectrum of the different variables and scenarios for each model, for the multi-model mean (hereafter MMM), and for the observational data. All figures show the logarithms to base 10 of the spectrum (accordingly, all figures showing differences between spectra correspond to the $\log_{10}$ of the ratio). For each spectrum, the total power is also calculated and included in Table 2. After analyzing the historical biases and the relationship between biases in U250 and in OLR, we analyze the future projections. We focus on the symmetric component of the spectrum while the ω-k spectra of the anti-symmetric component are included in Online Resource 2.

3 Changes in Tropical Spectrum

3.1 Historical Bias

Figure 1 shows the ω-k power spectra of the symmetric component of OLR in the historical simulations. Blue contours indicate regions in which the power exceeds the background spectrum by at least 20%, hence showing the power in the MJO and CCEWs that can be distinguished from the background turbu-

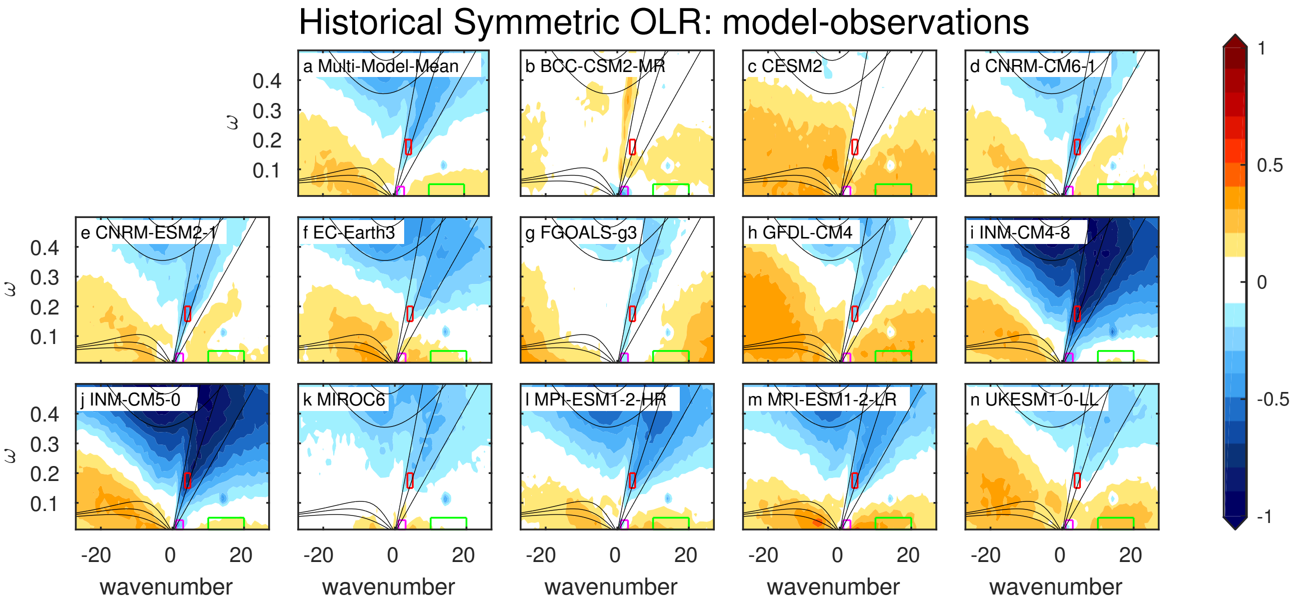

Fig. 2 Difference in the ω-k power spectra (log-scaled) of the symmetric component of raw OLR $(W/m^2)^2 \cdot s$: (a) MMM, and (b-o) individual models. Contour interval is 0.1. Black lines are the dispersion curves of equatorial waves for equivalent depths of 10m, 30m and 90m. Rectangles mark the areas for the correlation graphs shown later: green marks areas without a theoretical dry wave ($10 \leq k \leq 20$, $20 \leq T \leq 96$ days), magenta marks ω-k combinations in the vicinity of the MJO ($1 \leq k \leq 3$, $24 \leq T \leq 96$ days) and red marks ω-k combinations in the vicinity of the KW ($3.5 \leq k \leq 5$, $3.5 \leq T \leq 7$ days).

lent red-noise (Garfinkel et al, 2021), and such a ratio is statistically significant at the 95% level even in the relatively short observational record (Shamir et al, 2021). Observations clearly show power exceeding the background spectrum for ω-k combinations associated with the MJO, KW and lower wavenumber ER ($k \leq 8$), and so do many of the models. The MMM shows a generally good representation of the MJO, KW and ER, as compared to observations, as represented by the blue contour. The KW is simulated in most models, though not all models capture a realistic phase speed: in some models the KW propagates too slowly (e.g. both CNRM and FGOALS-g3) while in others it propagates too fast (e.g. EC-Earth3). If all of the individual model responses are averaged together to form the MMM, the KW phase speed is also too fast.

The fidelity of the MMM and of each model is more easily visualized by computing the bias with respect to observations, shown in Figure 2 (note that the bias is defined here as the difference between the log_{10} of the power spectra, i.e. the $\log_{10}$ of the ratio of modeled to observed power). BCC-CSM2-MR captures the spectrum most accurately. The remaining models, as well as the MMM, generally overestimate low frequencies except for low wavenumbers, and underestimate higher frequencies. The magnitude of the bias differs be-

Total power

model no.	model name	OLR bias	U250 bias	OLR SSP245	OLR SSP585	U250 SSP245	U250 SSP585
a	BCC-CSM2-MR	135.6	507.6	-18.5	-76.1	-119.8	-222.4
b	CESM2	346.3	224.4	22.1	-12.2	-77.9	-146.3
c	CNRM-CM6-1	-68.4	55.9	20.0	11.3	-110.2	-174.3
d	CNRM-ESM2-1	-51.5	39.7	33.7	31.5	-101.0	-159.8
e	EC-Earth3	-239.9	-242.2	74.3	155.2	2.3	-25.0
f	FGOALS-g3	53.6	-167.9	-16.7	-47.2	-107.2	-186.6
g	GFDL-CM4	216.2	-30.1	200.3	241.9	-27.5	-72.2
h	INM-CM4-8	-927.0	-770.8	-48.1	-93.2	-60.7	-96.0
i	INM-CM5-0	-885.0	-739.3	-66.6	-142.4	-27.5	-51.5
j	MIROC6	-327.1	35.8	-38.2	-59.9	-60.9	-89.5
k	MPI-ESM1-2-HR	-462.7	-8.2	14.2	-16.5	-70.8	-108.9
l	MPI-ESM1-2-LR	-339.2	0.4	-0.9	-20.4	-64.2	-103.1
m	UKESM1-0-LL	33.2	207.4	-74.4	-171.1	-155.1	-265.1
	MMM	-193.5	-21.9	7.8	-15.3	-75.4	-130.8

Table 2 Summary of total power of each model and MMM for OLR and U250: for bias and for the differences between future projections and historical assessments.

tween the models, and is particularly pronounced for the INM models (i.e., INM-CM4-8 and INM-CM5-0).

Similar to CMIP5, many models have a too-weak MJO bias, though in Figure 2 this bias is most notable in four models: BCC-CSM2-MR, FGOALS-g3, INM-CM4-8, INM-CM5-0. While the other models may simulate a reasonable amount of power for ω-k values associated with the MJO, these other models simulate too much power at low frequencies at other wavenumbers however, and hence the MJO is not as important at accounting for intraseasonal variability in essentially all (BCC-CSM2-MR the lone exception) models as compared to observations.

Biases for KW are even more common. On Figure 1, only two-thirds of the models simulate enhanced power above the background spectrum at ω-k combinations corresponding to the KW, with the INM, GFDL and MPI models struggling most. On Figure 2, we compare to observations rather than each model's background spectrum. Six models are reasonable (BCC-CSM2-MR, CESM2, EC-Earth3, GFDL-CM4, MIROC6 and UKESM1-0-LL), three slightly underestimate KW (CNRM-CM6-1, CNRM-ESM2-1, FGOALS-g3), and the remaining four (INM-CM4-8, INM-CM5-0, MPI-ESM1-2-HR, MPI-ESM1-2-LR) underestimate it by at least a factor of three ($= 10^{0.5}$).

In contrast to the MJO and KW, all of the models capture enhanced power for ER compared to each model's background spectrum in Figure 1. When compared to observations (Figure 2), FGOALS-g3 and MIROC6 simulate a realistic amount of ER power, most of the models overestimate it and BCC-CSM2-MR slightly underestimates it at low wavenumbers.

Table 2 shows the total power of the models compared to the observations (third column from the left). About half of the models have a negative total bias, while the others have a positive total bias. The absolute value of the total bias is smallest in UKESM1-0-LL, though this is the net of too-strong

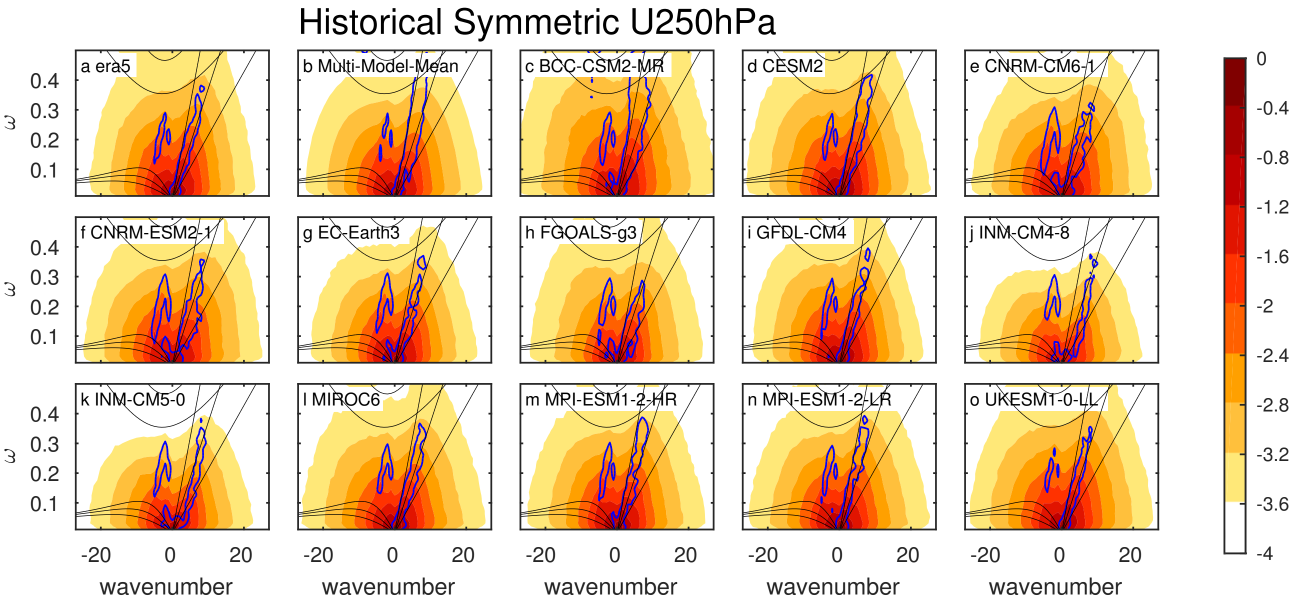

Fig. 3 $\log_{10}$ of the ω-k power spectra of the symmetric component of zonal wind $(m/s)^2 \cdot s$ at 250 hPa for all models and observations: (a) observations, (b) MMM, and (c-o) individual models. Contour interval is 0.4. Black lines are the dispersion curves of equatorial waves for equivalent depths of 10m, 30m and 90m. A blue contour indicates where the power exceeds the background by 35%.

low frequency and too-weak high frequency variability. The improvement of the OLR spectrum as compared to CMIP3 and CMIP5 models is discussed in later sections.

We now switch our focus to the U250 ω-k power spectra in the historical simulations (Figure 3). Compared to the OLR spectra, the symmetric component of historical U250 ω-k power spectra is more confined to lower wavenumbers and frequencies. While the enhanced power in the vicinity of the KW is clear, MJO and ER are less evident (the conclusion is unchanged if we lower the threshold for the blue contour on Figure 3, not shown). The power at negative low wavenumbers and frequencies of approximately 0.1-0.3 corresponds to the external Rossby-Haurwitz waves (Hendon and Wheeler, 2008), which are not in the scope of this study. Looking at the MMM spectrum, the total power and also the power associated with the KW is represented fairly realistically.

Looking at the U250 spectrum bias of the models relative to observations (Figure 4), there is a systematic tendency for too little power at low wavenumbers relative to larger wavenumbers, and also too much power at low frequencies and too little at high frequencies. The net effect is that for most models (the exceptions are BCC-CSM2-MR, CESM2, FGOALS-g3, and GFDL-CM4) spectrum biases take the form of a triangle. Some individual models also suffer

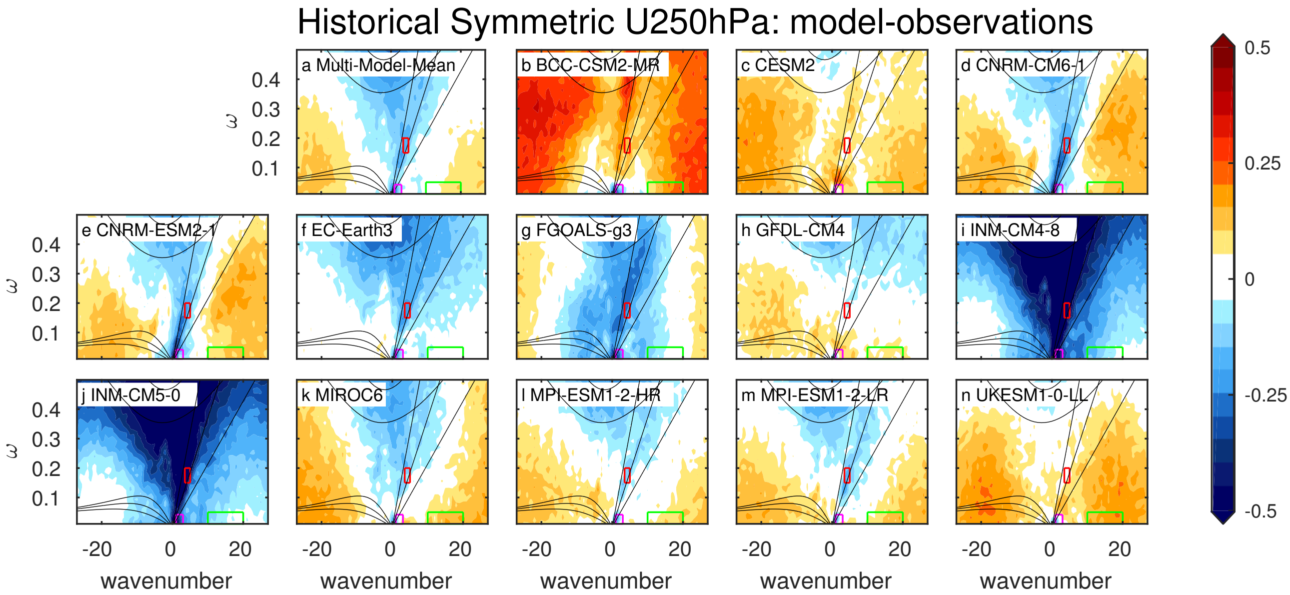

Fig. 4 Difference in the ω-k power spectra (log-scaled) of the symmetric component of raw zonal winds $(m/s)^2 \cdot s$ at 250 hPa: (a) MMM, and (b-o) individual models. Contour interval is 0.05. Black lines are the dispersion curves of equatorial waves for equivalent depths of 10m, 30m and 90m. Rectangles mark the areas for the correlation graphs (Figures 5, 7, 8): green marks areas without a theoretical dry wave ($10 \leq k \leq 20$, $20 \leq T \leq 96$ days), magenta marks ω-k combinations in the vicinity of the MJO ($1 \leq k \leq 3$, $24 \leq T \leq 96$ days) and red marks ω-k combinations in the vicinity of the KW ($3.5 \leq k \leq 5$, $3.5 \leq T \leq 7$ days).

from additional biases. BCC-CSM2-MR, CESM2 and UKESM1-0-LL have a positive bias for most of the spectrum (BCC-CSM2-MR particularly biased), while the bias of EC-Earth3, FGOALS-g3, INM-CM4-8 and INM-CM5-0 is mostly negative (INM-CM4-8 and INM-CM5-0 bias values are particularly low and are an outlier). The sum of the biases for all values of ω and k are lower however (see Table 2), because the total negative and positive biases within each spectrum compensate and cancel. Specifically, CNRM-CM6-1, CNRM-ESM2-1, MIROC6, MPI-ESM1-2-HR and MPI-ESM1-2-LR have a somewhat similar distribution of negative and positive bias, which is also reflected in the MMM spectrum. The bias in GFDL-CM4 differs from that in any other model, and appears to capture too much westward propagation and not enough eastward propagation. The main factor for the significant variability among the models is likely their differing convection schemes (see Online Resource 1). Another probable factor could be different representations of the background upper tropospheric winds, which affects tropical wave modes through more than just a simple Doppler filtering (De-Leon et al, 2022; Roundy, 2020a,b).

Most models have a too-weak MJO in U250, similar to the bias in OLR. Six models slightly underestimate it (BCC-CSM2-MR, CNRM-CM6-1, CNRM-

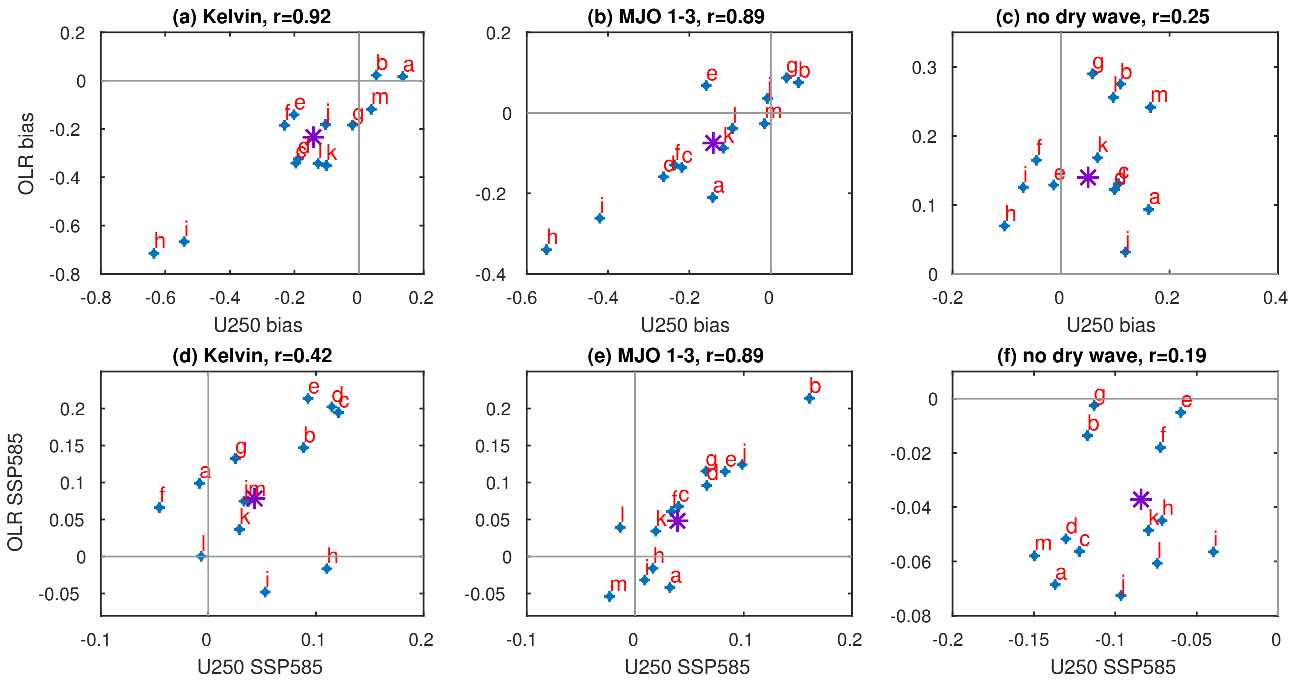

Fig. 5 Across model spread in the power spectra of OLR and zonal winds at 250 hPa in (a-c) historical biases and in (d-f) SSP585. ω-k values: (a,d) KW: $3.5 \leq k \leq 5$, $3.5 \leq T \leq 7$ days; (b,e) MJO: $1 \leq k \leq 3$, $24 \leq T \leq 96$ days; (c,f) no dry wave: $10 \leq k \leq 20$, $20 \leq T \leq 96$ days. See the boxed regions on Figure 2. Letters correspond to the labeling of the models on Table 2, and the purple star is the MMM. The correlation for each panel is indicated in its heading.

ESM2-1, EC-Earth3, MPI-ESM1-2-HR, MPI-ESM1-2-LR) and three more (FGOALS-g3, INM-CM4-8, INM-CM5-0) underestimate it by more than a factor of two $(= 10^{0.3})$. Note that those three also underestimate the MJO in OLR.

In order to better quantify the relationship between biases in U250 and OLR, we compare the biases in Figure 5a-c, and specifically use the average spectral-power within the colored rectangles on Figures 2 and 4. They represent regions of the ω-k spectrum associated with specific phenomena: red represents KW, magenta represents the MJO and green represents a region, with no theoretical dry wave (i.e., the background; Garfinkel et al, 2021). The phenomena are not confined into the boundaries of those areas, but the power values there are representative. We picked these relatively small regions because these regions include the wave modes for all of the models we consider. A broader region would lead to including regions in spectral space outside of the e.g. KW for at least one specific model. Note that although the KW band chosen is relatively small, it is more representative than other bands checked across all of the models (not shown).

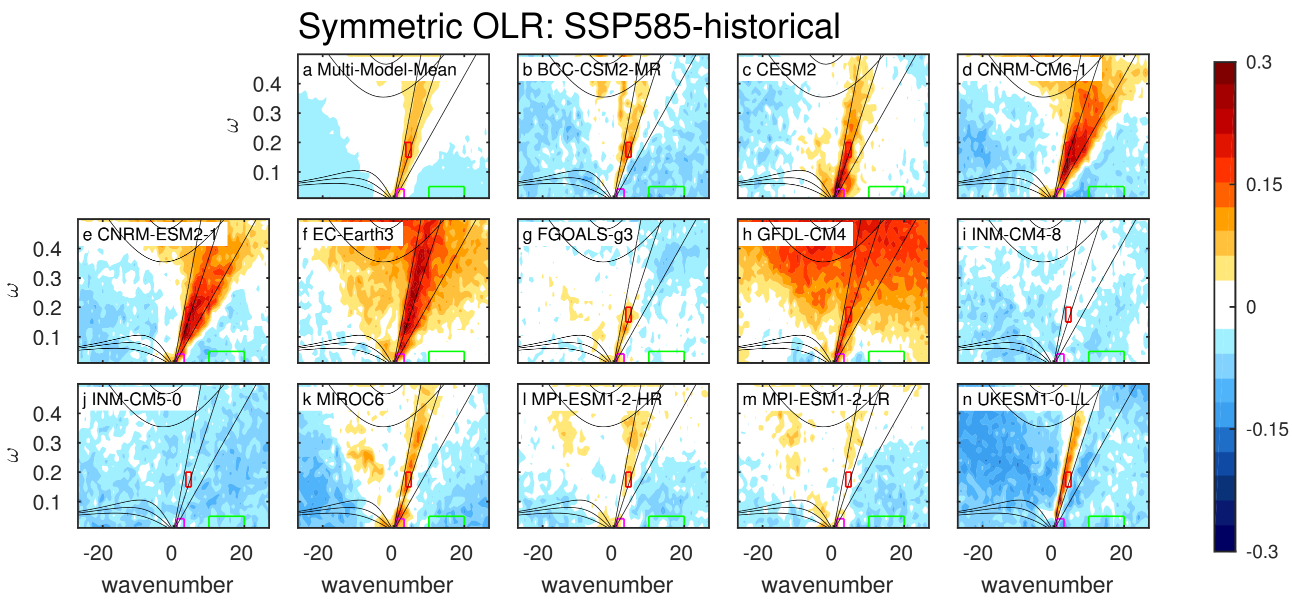

Fig. 6 Difference between the ω-k power spectra (log-scaled) of the SSP585 projection and historical simulation for the symmetric component of raw OLR $(W/m^2)^2 \cdot s$ data. (a) MMM, and (b-o) individual models. Contour interval is 0.05. Black lines are the dispersion curves of equatorial waves for equivalent depths of 10m, 30m and 90m. Rectangles mark the areas for the correlation graphs (Figures 5, 7, 8): green marks areas without a theoretical dry wave ($10 \leq k \leq 20$, $20 \leq T \leq 96$ days), magenta marks ω-k combinations in the vicinity of the MJO ($1 \leq k \leq 3$, $24 \leq T \leq 96$ days) and red marks ω-k combinations in the vicinity of the KW ($3.5 \leq k \leq 5$, $3.5 \leq T \leq 7$ days).

Figure 5a-c shows the correlations between the OLR and U250 biases in the chosen regions. The corresponding correlations between the raw data are similar (not shown). Although the OLR and U250 spectra differ in the redness of the spectra in wavenumber (i.e., the slope in k), and models with biases in the background spectra of one variable do not necessarily have a bias in the background spectra of the other (Figure 5c), there is a tight relationship between models that struggle to represent the MJO or the KW in OLR vs. those that struggle to represent them in U250 (correlation exceeding 0.85; Figure 5a,b). Out of the 13 models, two are noticeably poor: INM-CM4-8 and INM-CM5-0 (labeled as h and i). They stand out in both OLR and U250 spectra, with their significantly low values for both MJO and KW, and also for the total bias (as shown in Table 2). The other models have relatively low bias for KW and MJO at U250 (less than $10^{0.2}$ or 58%). Most models also do not have a significant bias for ER (not shown).

3.2 Future Assessments

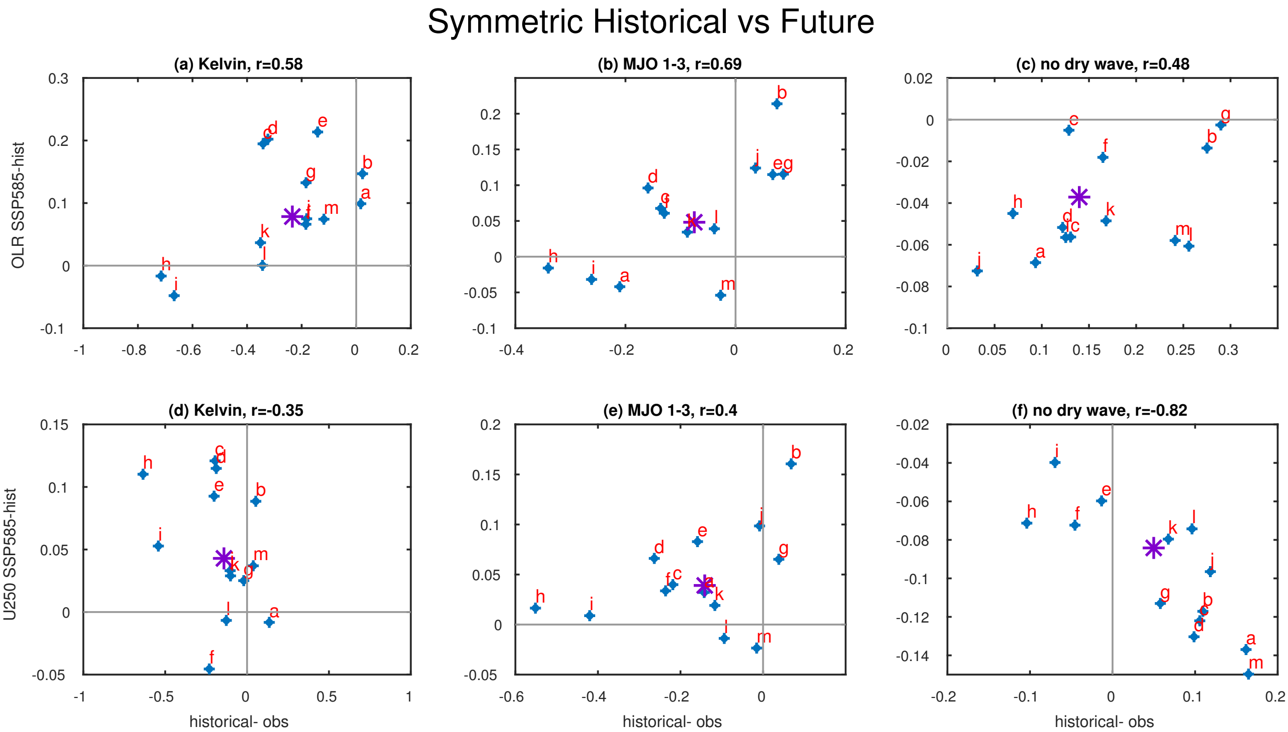

Fig. 7 Across model spread in projected changes (SSP585-historical) and historical bias of the models:(a-c) OLR, and (d-f) U250. ω-k values: (a, d) KW: $3.5 \leq k \leq 5$, $3.5 \leq T \leq 7$ days; (b, e) MJO: $1 \leq k \leq 3$, $24 \leq T \leq 96$ days; (c, f) no dry wave: $10 \leq k \leq 20$, $20 \leq T \leq 96$ days. See the boxed regions on Figure 2. Letters correspond to the labeling of the models on Table 2, and the purple star is the MMM. The correlation for each panel is indicated in its heading.

Section 3.1 established that most CMIP6 models (the INM models the lone exceptions) represent reasonably well the observed equatorial wave spectrum, which gives us confidence that their future projections may be of some value. We now analyze these future projections. Figure 6 presents the difference between the SSP585 future projection and the historical data for the symmetric component of the OLR spectra (see Online Resource 2 for U250 and for SSP245). Although the models have an overall decrease in power, all models except for two (INMs) project an intensification of KW. Most of them also project an increase in KW phase speed. The MJO strengthens slightly in most models. In contrast, variability at low frequencies and high wavenumbers is projected to weaken in almost all models (FGOALS-g3 the lone exception).

One might expect future projections to be more reliable in models that are capable of more reasonably capturing the present climate, and hence Figure 7 considers the relationship between historical biases and future changes (SSP585-historical) for both OLR and U250. While projections of KW intensification in OLR are even more pronounced in models with smaller historical biases (Figure 7a), no such effect is evident in U250 (Figure 7d): the correlation of historical biases and future changes for U250 is not statistically significant at the 95% level assuming each model is an independent degree of freedom. Note however that the same relationship is also evident for the SSP245 projections (see Online Resource 2), and if the two projections are treated as independent samples then the overall negative correlation for the KW for U250 would be significant. Future work with more models should revisit this apparent contradiction between OLR and U250 as to the connection between historical biases and future changes for KW.

MJO intensification is smaller in magnitude than KW intensification (Figure 7b,e). While most models project an intensification in OLR, BCC-CSM2-MR and UKESM1-0-LL project a weakening. In addition, U250 changes are smaller in most models than in OLR, though in most individual models and the MMM there is a slight strengthening even for U250. Also, models with larger biases in their historical representation of the MJO (i.e. the MJO is too weak) tend to simulate little future change (BCC-CSM2-MR, CNRM, FGOALS-g3, INM, MPI, UKESM1-0-LL), while models with smaller historical biases tend to simulate a future intensification of the MJO (CESM2, EC-Earth3, GFDL-CM4, MIROC6; Figure 7b,e). Finally, changes in ER for wavenumbers less than 5 are not robust for both OLR and U250, however for larger wavenumbers ER activity is projected to decrease in all models.

Next, we consider whether models with bigger changes in U250 also simulate bigger changes in OLR. Figure 5d-f contrasts projected changes in OLR and U250, with the correlation across models shown for each panel. Models simulating a future strengthening of the MJO as measured by OLR also project a future strengthening in U250 (Figure 5e), a connection that mirrors the relationship between historical biases (Figure 5b). Further, the strengthening of the MJO in OLR is, for most models, somewhat stronger than the strengthening for U250, consistent with the models considered by Maloney et al (2019) (see their figure 2) and with theoretical expectations that the MJO related precipitation strengthens more than the MJO related mass flux. For the KW, on the other hand, there is little relationship between models simulating a stronger future change in OLR to those simulating a stronger future change in U250 (Figure 5d). This might be partially due to differences in projected KW phase speeds, and partially because of the INM models, which stand out again.

All models show a decrease in total power in U250 (Table 2) in the SSP585 scenario, and all models except for one simulate a similar decrease in SSP245 (EC-Earth3). They all project a decrease in power in the background, at least to some extent, and an increase of power in low wavenumbers (mostly eastward, but also westward). In OLR, however, four models have an increase in total power (CNRM, EC-Earth3 and GFDL-CM4). Those models project the most intensification of KW and higher frequencies in the spectra. Still, they all project some decrease in at least lower-frequency-background (see Figure 6). As evident in Figures 6 and 7c,f, all models project at least some decrease in

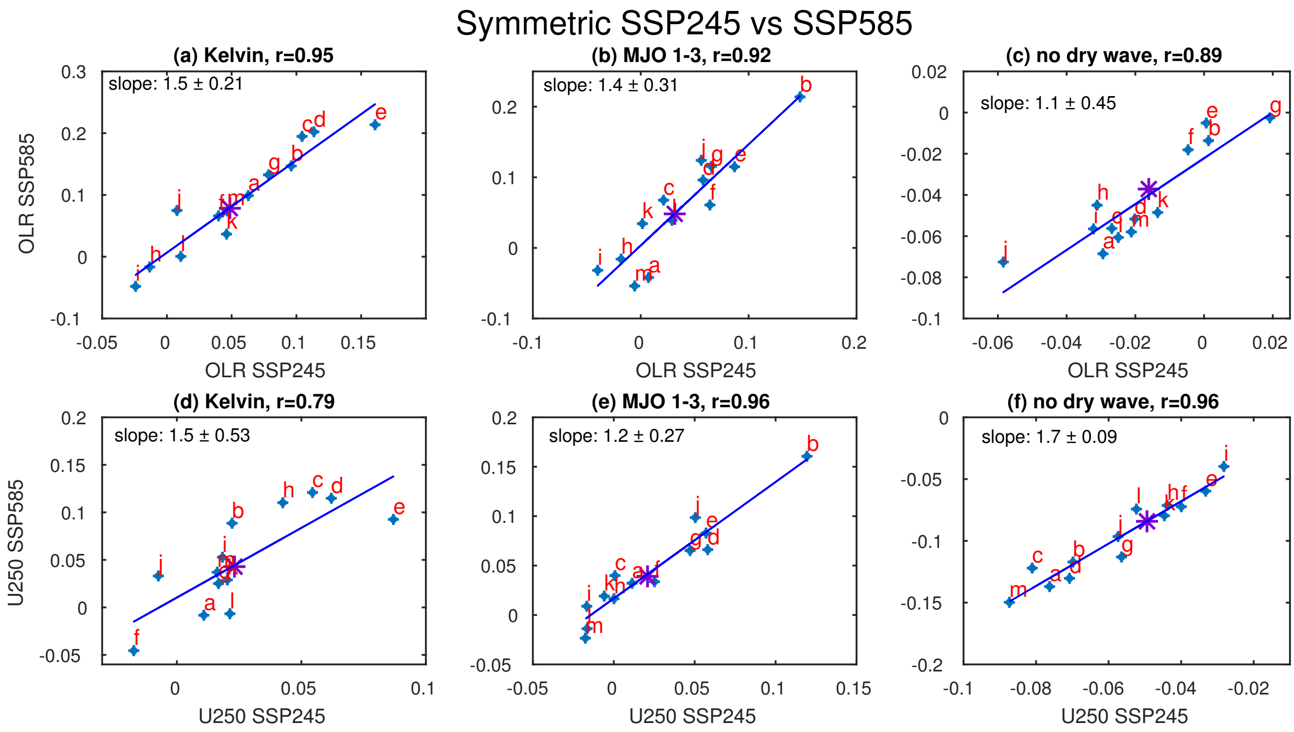

Fig. 8 Across model spread in future projected changes for the SSP245 and SSP585 scenarios:(a-c) OLR, and (d-f) U250. ω-k values: (a, d) KW: $3.5 \leq k \leq 5$, $3.5 \leq T \leq 7$ days; (b, e) MJO: $1 \leq k \leq 3$, $24 \leq T \leq 96$ days; (c, f) no dry wave: $10 \leq k \leq 20$, $20 \leq T \leq 96$ days. See the boxed regions on Figure 2. Letters correspond to the labeling of the models on Table 2, and the purple star is the MMM. A best-fit line and its slope, including 95% confidence intervals, are shown for each panel. The correlation for each panel is indicated in its heading.

background power in both OLR and U250, though there is little relationship between the magnitude of future reductions in the background in U250 vs OLR (Figure 5f). A weakening in the background power is to be expected if the background is driven by turbulent transfer from small-scale convection: total mass transport in the tropics is expected to weaken under climate change due to energetic constraints (Allan et al, 2020; Held and Soden, 2006), and this mass transport occurs within convective cells. Models with too-strong variance in U250 in their historical background spectrum tend to simulate a stronger weakening (Figure 7f), however this effect is not evident for OLR (Figure 7c).

Are the changes projected in SSP245 and in SSP585 linear, e.g. is the KW intensification in the SSP585 scenario approximately double that in the SSP245 scenario? We consider this by contrasting projected changes in SSP245 vs. SSP585 in Figure 8 for each model. It is evident that there is a strong connection between the future projections, and a model with a stronger response for SSP245 also simulates a stronger response for SSP585. The correlation between future projections in SSP245 and in SSP585 is above 0.85 in almost all regions (Figure 8). Both OLR and U250 KW have a slope of 1.5 (Figure 8a,d), OLR MJO has a slope of 1.4 (Figure 8b) and U250 background has a slope of 1.7 (Figure 8f). Those slopes are somewhat proportional to the respective focings. However, the slopes for U250 MJO and OLR background are not proportional with the underlying forcing (just 1.2 and 1.1 respectively; Figure 8e,c), though the reduction in the slope as compared to the other panels is not statistically significant. The connection of these slopes to the radiative forcings and changes in convective mass transport in SSP245 vs SSP585 should be a subject for future research.

4 Summary and Discussion

Assessing future change of the MJO and CCEWs is important both for their local tropical influence and their teleconnections to the extratropics. In this study we analyzed simulations of the MJO, KW and ER in 13 CMIP6 models, for U250 and OLR and three scenarios.

We began by considering whether these models realistically simulate the tropical wave spectrum in their historical simulations. While the spectra of U250 and OLR differ in the background spectrum, for the ω-k combinations of the wave-modes, models' performance for the historical simulation in, e.g., U250 is robustly related to performance in OLR. For both U250 and OLR, most models underestimate the power associated with the MJO and KW, and overestimate the power associated with ER. The KW bias is most significant, and it is not always simulated at a realistic phase speed. On the other hand, ER biases are generally small.

Out of the thirteen models, two (INM-CM4-8, INM-CM5-0) are noticeably poorer than the rest. This is probably due to their outdated convection scheme, which appears to have not been materially updated since the 1980s (Volodin et al, 2017). Seven other models can be compared to their earlier versions contributed to CMIP3, as analyzed by Lin et al (2006) (CESM2, CNRM-CM6-1, CNRM-ESM2-1, GFDL-CM4, MIROC6, MPI-ESM1-2-HR and MPI-ESM1-2-LR). During the past years, the models have been improved in different ways, including various aspects of their atmospheric component: radiation, aerosols, resolution and microphysics. The convection schemes of all of those models have received much attention and were improved significantly, mostly between CMIP5 and CMIP6 (except for MIROC, which shows significantly better results already in CMIP5), and it is known that CCEWs are particularly sensitive to the convective scheme (Frierson et al, 2011). As suggested in section 3.1, the latest versions of the models perform significantly better than their earlier versions, to the extent that they are comparable to observations. Further details and references about the models are available in Online Resource 1.

After establishing that most models qualitatively, if not quantitatively, resemble observations we examined the future projections for SSP245 and SSP585 scenarios. We focused on the SSP585 scenario, which has more significant change, though results are generally similar for SSP245. Eleven out of the thirteen models project a clear intensification of KW relative to their historical simulation. The other two are the poorer-performing INM models. In addition to the intensification of KW, the models project that KW phase speeds will also increase, in accordance with the stabilization of the tropics and enhanced warming aloft which will lead to a larger gross moist stability (GMS) and hence deeper equivalent depths (Frierson et al, 2011). In contrast, the background spectra for essentially all ω-k values and for larger-wavenumber ER is projected to weaken. Projected changes in the ER for small wavenumbers are less pronounced.

The MJO strengthens slightly in the MMM and crucially also in U250 in models which simulate a more realistic MJO in the historical climate. This projection appears to stand in contrast to other studies indicating a weak change in the zonal winds of the MJO, especially compared to the significant projected increase in precipitation (Jiang et al, 2020; Maloney et al, 2019; Chang et al, 2015). Furthermore, the gap between the MJO and KW grows as the KW shifts to higher phase speeds, and the background spectrum in the vicinity of the MJO weakens. The net effect is a more organized tropical circulation on intraseasonal timescales that may affect other phenomena in, say, the extratropics.

These results support previous work that has found that the MJO will strengthen due to enhanced frictional moisture convergence, nonlinear wind-induced surface heat exchange, and vertical advection of moist static energy (Jiang et al, 2020; Maloney et al, 2019; Arnold et al, 2015; Liu et al, 2013). This previous work focused more on the MJO than the KW, however we find the KW intensification to be more robust. Future work should consider why these mechanisms act to preferentially intensify the KW more than the MJO, and why they do not act to intensify other modes such as inertia-gravity waves or equatorial Rossby waves. One possible mechanism is that the strengthening of the subtropical jet in response to climate change leads to more eastward propagating subtropical wave-modes as compared to westward. To the extent that Kelvin waves are excited by subtropical variability propagating into the tropics, this should lead to more KW at the expense of other wave-modes. Ongoing work is aimed at testing this hypothesis, and results will be reported in a future publication.

Nevertheless, this projected strengthening is not uniformly simulated by all models nor are changes in SSP245 vs. SSP585 proportional to the underlying radiative forcing, and more detailed investigation is needed into how the structure of the MJO (e.g., amplitude, regions of growth/decay) will change. Moreover, further work should examine more closely the band between the MJO and KW, especially regarding different interpretations of the power spectrum (Garfinkel et al, 2021; Roundy, 2020b). In addition, future work should investigate whether this relative strengthening of the power of the MJO may affect its influence on the extratropics and potentially lead to improved forecast abilities.

5 Statements and Declarations

All authors contributed to the study conception and design. Material preparation and data were provided by Jian Rao and Ofer Shamir. Ofer Shamir began the data analysis, and Hagar Bartana performed most of the data analysis. Chaim Garfinkel oversaw the project. The first draft of the manuscript was written by Hagar Bartana and all authors commented on previous versions of the manuscript. All authors read and approved the final manuscript. C. I. G. and H. B. are supported by the ISF-NSFC joint research program (grant No.3259/19) and by the European Research Council starting grant under the European Union's Horizon 2020 research and innovation program (Grant Agreement 677756). Jian Rao is supported by the National Natural Science Foundation of China (42175069). The authors have no competing interests to declare that are relevant to the content of this article.

Acknowledgements Interpolated OLR data provided by the NOAA/OAR/ESRL PSL, Boulder, Colorado, USA, from their Web site at `https://psl.noaa.gov/data/gridded/data.interp_OLR.html`. CMIP6 data is available from the ESGF website at `https://esgf-node.llnl.gov/projects/cmip6/`. Correspondence should be addressed to C.I.G. (email: chaim.garfinkel@mail.huji.ac.il). The authors thank Paul Roundy and the two anonymous reviewers for their constructive comments.
The datasets analysed during the current study are available in the ESGF repository, `https://esgf-node.llnl.gov/projects/cmip6/`

References

Ahn MS, Kim D, Sperber KR, Kang IS, Maloney E, Waliser D, Hendon H (2017) Mjo simulation in cmip5 climate models: Mjo skill metrics and process-oriented diagnosis. Climate Dynamics 49(11):4023–4045

Ahn MS, Kim D, Kang D, Lee J, Sperber KR, Gleckler PJ, Jiang X, Ham YG, Kim H (2020) Mjo propagation across the maritime continent: Are cmip6 models better than cmip5 models? Geophysical Research Letters 47(11):e2020GL087,250

Allan RP, Barlow M, Byrne MP, Cherchi A, Douville H, Fowler HJ, Gan TY, Pendergrass AG, Rosenfeld D, Swann AL, et al (2020) Advances in understanding large-scale responses of the water cycle to climate change. Annals of the New York Academy of Sciences 1472(1):49–75

Arnold NP, Branson M, Kuang Z, Randall DA, Tziperman E (2015) Mjo intensification with warming in the superparameterized cesm. Journal of Climate 28(7):2706–2724

Bui HX, Maloney ED (2019) Transient response of mjo precipitation and circulation to greenhouse gas forcing. Geophysical Research Letters 46(22):13,546–13,555

Chang CWJ, Tseng WL, Hsu HH, Keenlyside N, Tsuang BJ (2015) The madden-julian oscillation in a warmer world. Geophysical research letters 42(14):6034–6042

Danabasoglu G, Lamarque JF, Bacmeister J, Bailey D, DuVivier A, Edwards J, Emmons L, Fasullo J, Garcia R, Gettelman A, et al (2020) The community earth system model version 2 (cesm2). Journal of Advances in Modeling Earth Systems 12(2)

De-Leon Y, Garfinkel CI, Paldor N (2022) Waves on the equatorial β-plane in the presence of a uniform zonal flow: Beyond the doppler shift. Physics of Fluids 34(4):046,603

Döscher R, Acosta M, Alessandri A, Anthoni P, Arneth A, Arsouze T, Bergmann T, Bernadello R, Bousetta S, Caron LP, et al (2021) The ec-earth3 earth system model for the climate model intercomparison project 6. Geoscientific Model Development Discussions pp 1–90

Dunne J, Horowitz L, Adcroft A, Ginoux P, Held I, John J, Krasting J, Malyshev S, Naik V, Paulot F, et al (2020) The gfdl earth system model version 4.1 (gfdl-esm 4.1): Overall coupled model description and simulation characteristics. Journal of Advances in Modeling Earth Systems 12(11):e2019MS002,015

Frierson DM, Kim D, Kang IS, Lee MI, Lin J (2011) Structure of agcm-simulated convectively coupled kelvin waves and sensitivity to convective parameterization. Journal of the atmospheric sciences 68(1):26–45

Garfinkel CI, Fouxon I, Shamir O, Paldor N (2017) Classification of eastward propagating waves on the spherical earth. Quarterly Journal of the Royal Meteorological Society 143(704):1554–1564

Garfinkel CI, Shamir O, Fouxon I, Paldor N (2021) Tropical background and wave spectra: Contribution of wave–wave interactions in a moderately non-linear turbulent flow. Journal of the Atmospheric Sciences 78(6):1773–1789

Held IM, Soden BJ (2006) Robust responses of the hydrological cycle to global warming. Journal of climate 19(21):5686–5699

Hendon HH, Wheeler MC (2008) Some space–time spectral analyses of tropical convection and planetary-scale waves. Journal of the atmospheric sciences 65(9):2936–2948

Hersbach H, Bell B, Berrisford P, Hirahara S, Horányi A, Muñoz-Sabater J, Nicolas J, Peubey C, Radu R, Schepers D, Simmons A, Soci C, Abdalla S, Abellan X, Balsamo G, Bechtold P, Biavati G, Bidlot J, Bonavita M, De Chiara G, Dahlgren P, Dee D, Diamantakis M, Dragani R, Flemming J, Forbes R, Fuentes M, Geer A, Haimberger L, Healy S, Hogan RJ, Hólm E, Janisková M, Keeley S, Laloyaux P, Lopez P, Lupu C, Radnoti G, de Rosnay P, Rozum I, Vamborg F, Villaume S, Thépaut JN (2020) The era5 global reanalysis. Quarterly Journal of the Royal Meteorological Society n/a(n/a), DOI 10.1002/qj.3803, URL `https://rmets.onlinelibrary.wiley.com/doi/abs/10.1002/qj.3803`, `https://rmets.onlinelibrary.wiley.com/doi/pdf/10.1002/qj.3803`

Hoskins BJ, Karoly DJ (1981) The steady linear response of a spherical atmosphere to thermal and orographic forcing. Journal of Atmospheric Sciences 38(6):1179–1196

Huang P, Chou C, Huang R (2013) The activity of convectively coupled equatorial waves in cmip3 global climate models. Theoretical and applied climatology 112(3):697–711

Hung MP, Lin JL, Wang W, Kim D, Shinoda T, Weaver SJ (2013) Mjo and convectively coupled equatorial waves simulated by cmip5 climate models. Journal of Climate 26(17):6185–6214

Jenney AM, Randall DA, Barnes EA (2021) Drivers of uncertainty in future projections of madden–julian oscillation teleconnections. Weather and Climate Dynamics 2(3):653–673

Jiang X, Waliser DE, Xavier PK, Petch J, Klingaman NP, Woolnough SJ, Guan B, Bellon G, Crueger T, DeMott C, et al (2015) Vertical structure and physical processes of the madden-julian oscillation: Exploring key model physics in climate simulations. Journal of Geophysical Research: Atmospheres 120(10):4718–4748

Jiang X, Adames ÁF, Kim D, Maloney ED, Lin H, Kim H, Zhang C, DeMott CA, Klingaman NP (2020) Fifty years of research on the madden-julian oscillation: Recent progress, challenges, and perspectives. Journal of Geophysical Research: Atmospheres 125(17):e2019JD030,911

Kiladis GN, Wheeler MC, Haertel PT, Straub KH, Roundy PE (2009) Convectively coupled equatorial waves. Reviews of Geophysics 47(2)

Le PV, Guilloteau C, Mamalakis A, Foufoula-Georgiou E (2021) Underestimated mjo variability in cmip6 models. Geophysical Research Letters 48(12):e2020GL092,244

Li L, Yu Y, Tang Y, Lin P, Xie J, Song M, Dong L, Zhou T, Liu L, Wang L, et al (2020) The flexible global ocean-atmosphere-land system model grid-point version 3 (fgoals-g3): description and evaluation. Journal of Advances in Modeling Earth Systems 12(9):e2019MS002,012

Liebmann B, Smith CA (1996) Description of a complete (interpolated) outgoing longwave radiation dataset. Bulletin of the American Meteorological Society 77(6):1275–1277

Lin JL, Kiladis GN, Mapes BE, Weickmann KM, Sperber KR, Lin W, Wheeler MC, Schubert SD, Del Genio A, Donner LJ, et al (2006) Tropical intraseasonal variability in 14 ipcc ar4 climate models. part i: Convective signals. Journal of climate 19(12):2665–2690

Liu P, Li T, Wang B, Zhang M, Luo Jj, Masumoto Y, Wang X, Roeckner E (2013) Mjo change with a1b global warming estimated by the 40-km echam5. Climate Dynamics 41(3):1009–1023

Madden RA, Julian PR (1972) Description of global-scale circulation cells in the tropics with a 40–50 day period. Journal of Atmospheric Sciences 29(6):1109–1123

Maloney ED, Adames ÁF, Bui HX (2019) Madden–julian oscillation changes under anthropogenic warming. Nature Climate Change 9(1):26–33

Matsuno T (1966) Quasi-geostrophic motions in the equatorial area. Journal of the Meteorological Society of Japan Ser II 44(1):25–43

Mauritsen T, Bader J, Becker T, Behrens J, Bittner M, Brokopf R, Brovkin V, Claussen M, Crueger T, Esch M, et al (2019) Developments in the mpi-m earth system model version 1.2 (mpi-esm1. 2) and its response to increasing co2. Journal of Advances in Modeling Earth Systems 11(4):998–1038

Meinshausen M, Nicholls ZR, Lewis J, Gidden MJ, Vogel E, Freund M, Beyerle U, Gessner C, Nauels A, Bauer N, et al (2020) The shared socio-economic pathway (ssp) greenhouse gas concentrations and their extensions to 2500. Geoscientific Model Development 13(8):3571–3605

Müller WA, Jungclaus JH, Mauritsen T, Baehr J, Bittner M, Budich R, Bunzel F, Esch M, Ghosh R, Haak H, et al (2018) A higher-resolution version of the max planck institute earth system model (mpi-esm1. 2-hr). Journal of Advances in Modeling Earth Systems 10(7):1383–1413

Paldor N (2015) Shallow water waves on the rotating Earth. Springer

Paldor N, De-Leon Y, Shamir O (2013) Planetary (rossby) waves and inertia–gravity (poincaré) waves in a barotropic ocean over a sphere. Journal of Fluid Mechanics 726:123–136

Raghavendra A, Roundy PE, Zhou L (2019) Trends in tropical wave activity from the 1980s to 2016. Journal of Climate 32(5):1661–1676

Rao J, Garfinkel CI, Chen H, White IP (2019) The 2019 new year stratospheric sudden warming and its real-time predictions in multiple s2s models. Journal of Geophysical Research: Atmospheres 124(21):11,155–11,174

Rao J, Garfinkel CI, White IP, Schwartz C (2020) The southern hemisphere minor sudden stratospheric warming in september 2019 and its predictions in s2s models. Journal of Geophysical Research: Atmospheres 125(14):e2020JD032,723

Rao J, Garfinkel CI, Wu T, Lu Y, Lu Q, Liang Z (2021) The january 2021 sudden stratospheric warming and its prediction in subseasonal to seasonal models. Journal of Geophysical Research: Atmospheres p e2021JD035057

Roundy PE (2020a) The association between the phase speed of the madden–julian oscillation and atmospheric circulation. In: The Multiscale Global Monsoon System, World Scientific, pp 301–314

Roundy PE (2020b) Interpretation of the spectrum of eastward-moving tropical convective anomalies. Quarterly Journal of the Royal Meteorological Society 146(727):795–806

Samarasinghe SM, Connolly C, Barnes EA, Ebert-Uphoff I, Sun L (2021) Strengthened causal connections between the mjo and the north atlantic with climate warming. Geophysical Research Letters 48(5):e2020GL091,168

Sardeshmukh PD, Hoskins BJ (1988) The generation of global rotational flow by steady idealized tropical divergence. Journal of the Atmospheric Sciences 45(7):1228–1251

Schwartz C, Garfinkel CI (2020) Troposphere-stratosphere coupling in subseasonal-to-seasonal models and its importance for a realistic extratropical response to the madden-julian oscillation. Journal of Geophysical Research: Atmospheres 125(10):e2019JD032,043

Séférian R, Nabat P, Michou M, Saint-Martin D, Voldoire A, Colin J, Decharme B, Delire C, Berthet S, Chevallier M, et al (2019) Evaluation of cnrm earth system model, cnrm-esm2-1: Role of earth system processes in present-day and future climate. Journal of Advances in Modeling Earth Systems 11(12):4182–4227

Sellar AA, Jones CG, Mulcahy JP, Tang Y, Yool A, Wiltshire A, O'Connor FM, Stringer M, Hill R, Palmieri J, Woodward S, de Mora L, Kuhlbrodt T, Rumbold ST, Kelley DI, Ellis R, Johnson CE, Walton J, Abraham NL, Andrews MB, Andrews T, Archibald AT, Berthou S, Burke E, Blockley E, Carslaw K, Dalvi M, Edwards J, Folberth GA, Gedney N, Griffiths PT, Harper AB, Hendry MA, Hewitt AJ, Johnson B, Jones A, Jones CD, Keeble J, Liddicoat S, Morgenstern O, Parker RJ, Predoi V, Robertson E, Siahaan A, Smith RS, Swaminathan R, Woodhouse MT, Zeng G, Zerroukat M (2019) Ukesm1: Description and evaluation of the u.k. earth system model. Journal of Advances in Modeling Earth Systems 11(12):4513–4558, DOI 10.1029/2019MS001739

Seo KH, Lee HJ (2017) Mechanisms for a pna-like teleconnection pattern in response to the mjo. Journal of the Atmospheric Sciences 74(6):1767–1781

Seo KH, Choi JH, Han SD (2012) Factors for the simulation of convectively coupled kelvin waves. Journal of climate 25(10):3495–3514

Shamir O, Schwartz C, Garfinkel CI, Paldor N (2021) The power distribution between symmetric and antisymmetric components of the tropical wavenumber–frequency spectrum. Journal of the Atmospheric Sciences 78(6):1983–1998

Stan C, Zheng C, Chang EKM, Domeisen DI, Garfinkel CI, Jenney AM, Kim H, Lim YK, Lin H, Robertson A, et al (2022) Advances in the prediction of mjo-teleconnections in the s2s forecast systems. Bulletin of the American Meteorological Society

Tatebe H, Ogura T, Nitta T, Komuro Y, Ogochi K, Takemura T, Sudo K, Sekiguchi M, Abe M, Saito F, et al (2019) Description and basic evaluation of simulated mean state, internal variability, and climate sensitivity in miroc6. Geoscientific Model Development 12(7):2727–2765

Vitart F (2017) Maddenjulian oscillation prediction and teleconnections in the s2s database. Quarterly Journal of the Royal Meteorological Society 143(706):2210–2220

Voldoire A, Saint-Martin D, Sénési S, Decharme B, Alias A, Chevallier M, Colin J, Guérémy JF, Michou M, Moine MP, et al (2019) Evaluation of cmip6 deck experiments with cnrm-cm6-1. Journal of Advances in Modeling Earth Systems 11(7):2177–2213

Volodin E, Mortikov E, Kostrykin S, Galin VY, Lykossov V, Gritsun A, Diansky N, Gusev A, Iakovlev N (2017) Simulation of the present-day climate with the climate model inmcm5. Climate dynamics 49(11):3715–3734

Wang L, Li T (2017) Convectively coupled kelvin waves in cmip5 coupled climate models. Climate Dynamics 48(3-4):767–781

Wheeler M, Kiladis GN (1999) Convectively coupled equatorial waves: Analysis of clouds and temperature in the wavenumber–frequency domain. Journal of Atmospheric Sciences 56(3):374–399

Wu T, Lu Y, Fang Y, Xin X, Li L, Li W, Jie W, Zhang J, Liu Y, Zhang L, et al (2019) The beijing climate center climate system model (bcc-csm): The main progress from cmip5 to cmip6. Geoscientific Model Development 12(4):1573–1600

Yoo C, Lee S, Feldstein SB (2012) Mechanisms of arctic surface air temperature change in response to the madden–julian oscillation. Journal of Climate 25(17):5777–5790

Zhang C (2005) Madden-julian oscillation. Reviews of Geophysics 43(2)

Supplementary Files

This is a list of supplementary files associated with this preprint. Click to download.

- onlineresource1.pdf
- onlineresource2.pdf
- Responsetoreviewers.pdf